Polyaniline-Grafted Reduced Graphene Oxide for Efficient Electrochemical Supercapacitors

Nanjundan Ashok Kumar,[†,§] Hyun-Jung Choi,[†] Yeon Ran Shin,[†] Dong Wook Chang,[†] Liming Dai,[‡] and Jong-Beom Baek[†,*]

[†]Interdisciplinary School of Green Energy/Institute of Advanced Materials & Devices, Ulsan National Institute of Science and Technology (UNIST), 100, Banyeon, Ulsan, 689-798, South Korea, and [‡]Department of Chemical Engineering, Case Western Reserve University, 10900 Euclid Avenue, Cleveland, Ohio 44106, United States. [§]Present address: Institute for Nanoscience and Cryogenics, Commissariat à l'Énergie Atomique (CEA), 17 Rue des Martyrs, 38054, Grenoble, Cedex 9, France.

As a new form of carbon, the intriguing two-dimensional sheet of sp²-bonded, single-atom-thick graphene has drawn much attention owing to its exotic in-plane properties, such as high electric conductivity, flexibility, and mechanical strength.[1,2] These unique features offer great promise for many potential applications.[3−5] In particular, its high electrocatalytic activity makes graphene an alluring material for sensors[6] and electrochemical energy storage.[7−10] Moreover, certain functionalized graphene-based materials, including functionalized graphene/graphite oxide (GO), exhibit large surface-to-volume ratios. This, together with their superior chemical stability and a broad electrochemical window, renders them as attractive electrode materials for lithium ion batteries[11] and electrochemical supercapacitor electrodes.[12,13] They possess extraordinary electrochemical and mechanical properties comparable to or even better than their carbon nanotube counterparts. Ultracapacitors based on graphene[14,15] and even flexible papers of graphene/GO as the sole building block have been fabricated, which have stimulated great interest among the energy science community. Additionally, GO-based materials with tunable oxygen functionalities on their basal planes facilitate surface modification for making composites with other materials, such as conducting polymers.[16]

While a high electrical conductivity of materials is one of the most critical requirements for a myriad of applications, including energy-related devices, conducting polymers have generally been used to meet such a need. High surface carbon materials or noble metal oxides and conducting polymer composites have been and are still

ABSTRACT
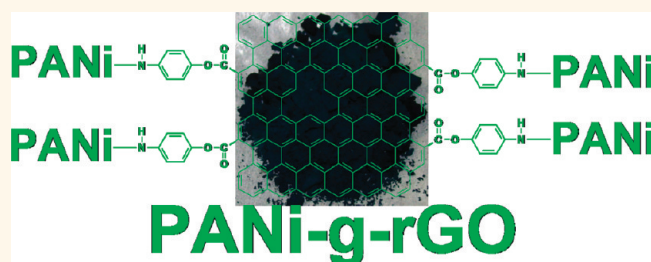
An alternative and effective route to prepare conducting polyaniline-grafted reduced graphene oxide (PANi-*g*-rGO) composite with highly enhanced properties is reported. In order to prepare PANi-*g*-rGO, amine-protected 4-aminophenol was initially grafted to graphite oxide (GO) *via* acyl chemistry where a concomitant partial reduction of GO occurred due to the refluxing and exposure of GO to thionyl chloride vapors and heating. Following the deprotection of amine groups, an *in situ* chemical oxidative grafting of aniline in the presence of an oxidizing agent was carried out to yield highly conducting PANi-*g*-rGO. Electron microscopic studies demonstrated that the resultant composite has fibrillar morphology with a room-temperature electrical conductivity as high as 8.66 S/cm and capacitance of 250 F/g with good cycling stability.

KEYWORDS: graphene oxide · exfoliation · polyaniline · composite · electrochemistry

being studied extensively today.[17] However, the poor conductivity and weak flexibility of some conducting polymers often limit them from usage in high-performance devices.[18] On the other hand, however, there has been much interest in polyaniline (PANi)-based materials for more than three decades simply because of their low cost and ease of synthesis.[19] Furthermore, PANi, being an excellent organic conductor with good environmental stability and biocompatibility,[20] has often been used to fabricate composites with carbonaceous materials for supercapacitor electrodes[21] and sensors.[20,3]
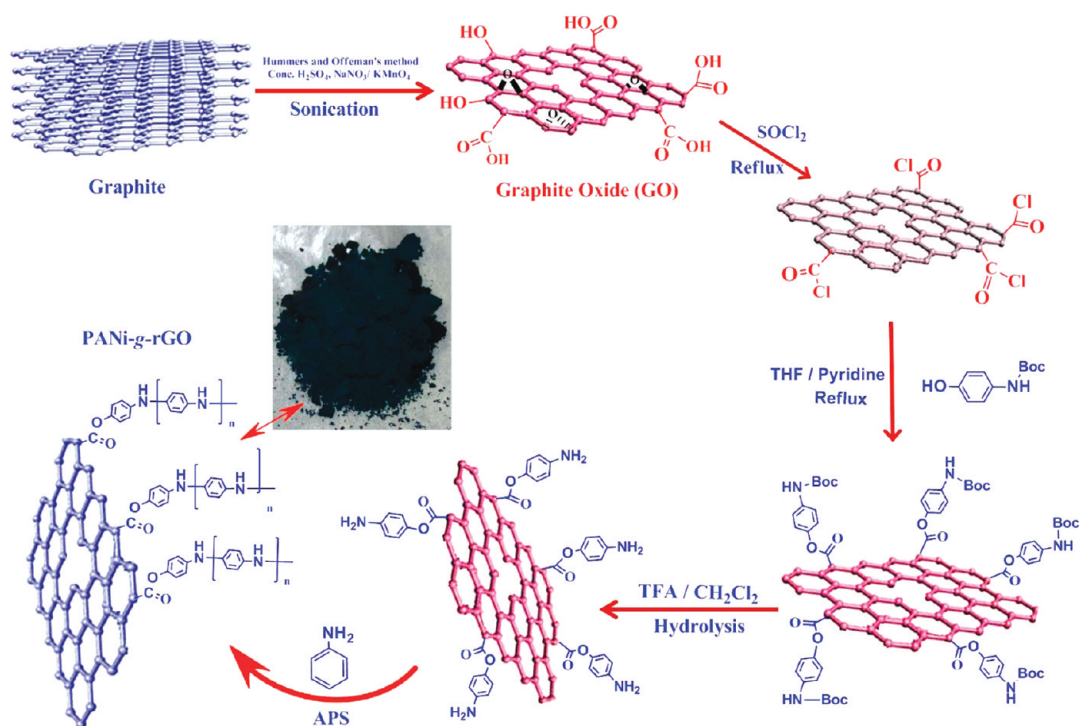
Figure 1. Schematic governing the preparation of PANi-*g*-rGO with a digital picture of the sample in the middle.

In this regard, the ability to hybridize carbon-based nanomaterials (namely, graphene/GO) with conducting polymers (*e.g.*, PANi) to produce composites has triggered burgeoning interest and is of great scientific and industrial importance.[5] In particular, graphene nanosheets (GNS) when compounded with conducting polymers can enhance not only the electrical conductivity but also the mechanical strength of resulting composites. These intriguing characteristics enable graphene-based conducting polymer composites to be prime candidates for energy applications and many others.[22,23] To date, extensive efforts and many approaches have been developed to prepare graphene-based composites, especially, GO-PANi or graphene-PANi composite powders, which have exhibited various functional properties.[24−27] Dramatic improvements in their properties have been achieved due to the synergistic effect between the two components composited through two main routes, *i.e.*, covalent grafting and noncovalent mixing/adsorption. Most of the prepared composite products have both pros and cons. Therefore, the effort for new methodologies to prepare hybrids with the aim of further enhancing the properties needs to be developed.

In this study, a novel route to prepare GO-based PANi composites in a three-step process starting from *N*-(*tert*-butoxycarbonyl)-4-aminophenol is established. Our strategy involves the covalent functionalization of amine-protected 4-aminophenol to acylated GO, which is subsequently polymerized in the presence of aniline monomer, thereby yielding highly conducting networks. Since the composite is covalently

functionalized and the GO was *in situ* reduced to a certain extent, the compatibility of reduced GO (rGO) with the PANi matrix is ensured, and hence phase separation is minimized. Furthermore, the inclusion of PANi is expected to maximize the unique potential of graphene. The formation of the heterostructures and their properties were systematically characterized using various analytical techniques.

RESULTS AND DISCUSSION

GO exhibits enormous active edges and oxygen functional groups on its basal plane, providing compatibility with polymer matrices when used as a host material in a composite. Moreover, the oxygen-containing functional groups on the surface of GO make it easily dispersible in aqueous solution and may also act as nucleation sites for producing PANi on its surfaces. The fabrication of PANi-grafted rGO (PANi-*g*-rGO) essentially includes three steps, as illustrated in Figure 1.

Initially, GO was produced from natural flake graphite (400 nm) by a modified Hummers and Offeman method,[28] in which GO existed in a mixture of single- and a few-layer structures in solution.[29] GO was further acylated in the presence of excess $SOCl_2$ and then reacted with amine-protected 4-aminophenol. The primary reason for selecting the amine-protected phenol derivative is to ensure that the covalent bonding between the acylated GO and the derivative happens through the hydroxyl groups present in the derivative and not through the amine moieties. Upon subsequent deprotection of *N*-(*tert*-butoxycarbonyl) groups by hydrolysis with trifluoroacetic acid, PANi-*g*-rGO was
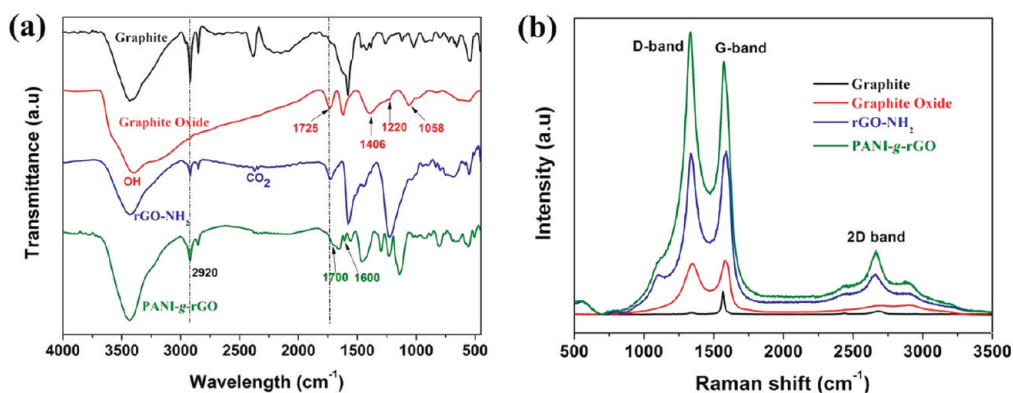
Figure 2. (a) FT-IR spectra and (b) Raman spectra of the samples.

prepared from *in situ* oxidative polymerization of aniline in the presence of an oxidant and amine-terminated rGO (rGO-NH$_2$) as an initiator. The resultant PANi-*g*-rGO glows a greenish color under ambient room light (Figure 1). On a whole, this kind of covalent surface functionalization strategy is similar to the well-known "graft-from" method to produce polymer brushes or coatings on any given surface. Compared to the covalent approach, the noncovalent approach may have many cons, such as slippage of the molecules, when compared to the covalent approach.[30,31]

FT-IR was used to elucidate the covalent grafting between the hydroxyl groups of *N*-(*tert*-butoxycarbonyl)aminophenol and the acyl-functionalized GO in this study. As can be seen in Figure 2a, the FT-IR spectrum of GO shows a strong absorption band at 1725 cm^{-1} due to the C=O stretching in the −COOH groups. It also exhibits a sharp band around 1622 cm^{-1} attributable to the vibrations of the residual water. Vibrational bands due to carboxy (C−O; 1406 cm^{-1}), epoxy (C−O; 1220 cm^{-1}), and alkoxy (C−O; 1058 cm^{-1}) groups situated at the edges of the GO nanosheets were also found, as reported elsewhere.[32] After the functionalization process and deprotection of *N*-(*tert*-butoxycarbonyl) groups by hydrolysis, rGO-NH$_2$ shows the presence of strong bands at around 1221 and 1725 cm^{-1}, characteristic of C−O and C=O, respectively, associated with the stretching modes of the ester linkages between the acyl-functionalized GO and the aminophenol derivative, suggesting a covalent linkage. Compared with GO, however, several new peaks attributed to PANI appeared in the spectrum of PANi-*g*-rGO. Notably, two new peaks around 1600 and 1461 cm^{-1} are attributed to the vibrations of C=N and C=C, respectively.[33,34] In addition, a stretching band assigned to C−N also appears at 1300 cm^{-1}. A band at about 800 cm^{-1} could be attributed to the C−H out-of-plane bending vibrations, while the many low-intensity peaks ranging from 780 to 580 cm^{-1} can be assigned to the vibrations of the C−H bonds in the benzene rings. The appearance of the quinonoid and benzenoid ring

vibrations (C=C stretching deformations) at about 1564 and 1461 cm^{-1}, respectively, clearly indicates the presence and formation of PANi on the graphene surfaces. As is commonly observed, the quinonoid band at 1564 cm^{-1} is less intense than the benzenoid band at 1461 cm^{-1}. The characteristic band attributable to the N−Q−N−Q stretch of the quinonoid ring was also found at around 1144 cm^{-1}, which clearly supports our hypothesis that the PANi has been covalently grafted onto the surface of the graphene sheets.

In conjunction with FT-IR spectroscopy, Raman scattering was measured to give a more complete picture of the chemical bonding structure.[35] As shown in Figure 2b, significant structural changes occurred during the chemical processing from natural graphite to GO, and the formation of PANi-*g*-rGO was reflected in the Raman spectra. As expected, the Raman scattering of the natural graphite displays a prominent G peak as the only feature, at 1590 cm^{-1}, corresponding to the first-order scattering of the E$_{2g}$ mode. On the other hand, however, the spectrum of the as-prepared GO displays two prominent peaks at 1350 and 1590 cm^{-1}, which correspond to the well-documented D mode or the phonon mode corresponding to the conversion of a sp^2-hybridized carbon to a sp^3-hybridized carbon and the G mode related to the vibration of a sp^2-hybridized carbon, respectively. It is worth noting that the intensity of the D band is slightly higher than the G band for the final compound due to the defects and partially disordered crystal structure of the graphene sheets, suggesting that the sheets have a high defect content, and also this phenomenon is noticed in most of the published results for all types of functionalized GO/GNS.[27] These defects might also be due to the smaller size of graphene sheets in the composites.[36] However, no obvious peaks arising from the PANi were observed, due probably to the peaks of PANi being too weak and/or overlapped with the GO peaks, as observed in a previous study.[36] Hence, FT-IR was employed to characterize the presence of PANi in the samples.
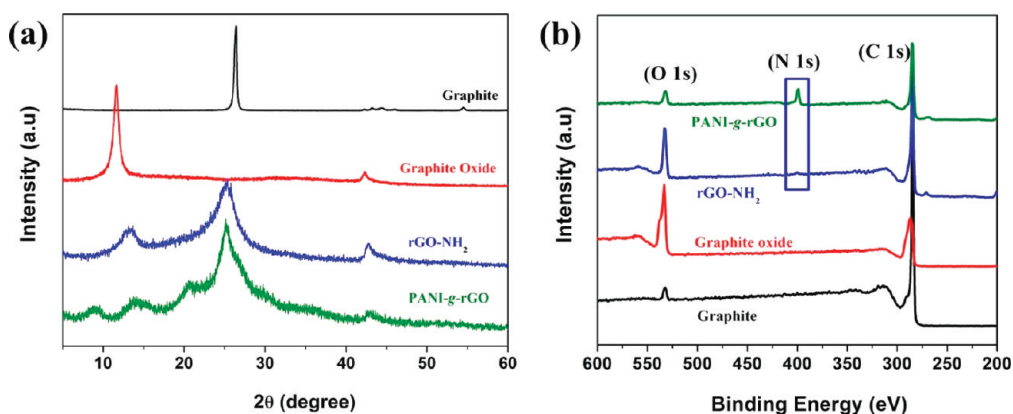
Figure 3. (a) Typical XRD patterns and (b) XPS spectra of the samples.

Since the aromatic structure in PANi are known to interact strongly with the plane of GO surfaces *via* pi-stacking and the Raman peaks of PANi superimposed on the carbon structures, the PANi-*g*-rGO has almost the same spectra as those of the rGO-NH$_2$. Meanwhile, the prominent 2D peak for the PANi-*g*-rGO can also be observed in the spectrum. From the 2D band of the PANi-*g*-rGO composite spectrum, it appears that the graphene in the composite consists of a variety of sheets varying from just a few layers up to five to ten layers,[37,38] as will be seen and discussed in detail in the following section on the morphology and layer information using HRTEM studies. The concomitant reduction of GO during the reaction with thionyl chloride (*in situ* thermal reduction and exposure to SOCl$_2$ vapors) is also evident from the increase in the 2D band, not only in the final grafted compound but also in rGO-NH$_2$, which agrees well with recent literature for the *in situ* reduction of GO.[39]

A wide-angle X-ray diffraction (WAXD) pattern of the powder samples was taken in order to estimate the degree of exfoliation that can be quantitatively estimated from the relative peak intensity. Figure 3a shows the XRD patterns of the pristine GO, revealing an intense and sharp peak centered at $2\theta = 11.66°$, corresponding to the interplanar spacing of GO sheets. This value can be assigned to the (001) reflection peak and might depend on the method of preparation and on the number of layers of water in the gallery space of the material.[40] In the case of rGO-NH$_2$, the peak of GO stacking disappeared and a new, broad, minor peak at 13.5° (011) and major peak at 25.4° (200) appeared instead, indicating that a significant portion of GO had been reduced. Similarly, the GO peak disappeared from PANi-*g*-rGO, implying that the GO had almost no aggregation and was fully utilized as the substrate of PANi to produce the composite hybrid. Additionally, the broad nature of the reflection in both rGO-NH$_2$ and PANi-*g*-rGO indicates poor ordering of the sheets along the stacking direction, implying that the samples could have been completely exfoliated to contain mostly a

single layer, a few layers, and/or even loosely stacked layers. The samples are clearly different from the crystalline pristine graphite, as also evidenced from the Raman scattering. The substantial shift of the (002) reflection during the processing of GO also confirms the formation of reduced graphene from GO. Three new broad peaks of PANi-*g*-rGO centered at $2\theta = 13°$ and 20.6° and the broad intense peak at around 25.1° corresponding to (011), (020), and (200) crystal planes are almost the same as that of pure PANi, which are also the characteristic Bragg diffraction peaks of the polymer.[41] Interestingly, for the PANi-*g*-rGO, we observed a weak and broad peak appearing nearly at $2\theta = 8°$, which is lower than that of GO. This could imply that the interplanar spacing of the PANi-*g*-rGO composite was broadened due to possible intercalation of PANi and that the rGO was fully exfoliated by treatment with PANi. Therefore, the XRD patterns further confirm the formation of PANi grafting on the surfaces of the rGO. The result is consistent with that of FT-IR and Raman investigations. To provide further insight and clear evidence for the formation of functionalized GNS from GO during the process, the samples were characterized by X-ray photoelectron spectroscopy (XPS), as shown in Figure 3b.

The spectra of the parent graphite powders, GO, and the PANi-*g*-rGO hybrid indicate the considerable degree of oxidation for GO and the subsequent reduction of GO to a certain extent in the final compound. The small amount of O 1s peak found in the final product might be due to the surface-adsorbed oxygen, which is also a common phenomenon, as noticed in the case of parent graphite as well.[42] It is generally believed that the decreased oxygen content may increase the sp^2 carbons on the graphene sheets,[43] leading to the increase of the $\pi-\pi$ interaction between graphene and PANi chains, which may facilitate the electron transfer and bring a synergistic effect to the electrochemical properties of the hybrid material. Compared with GO, the presence of a N 1s core level peak in the
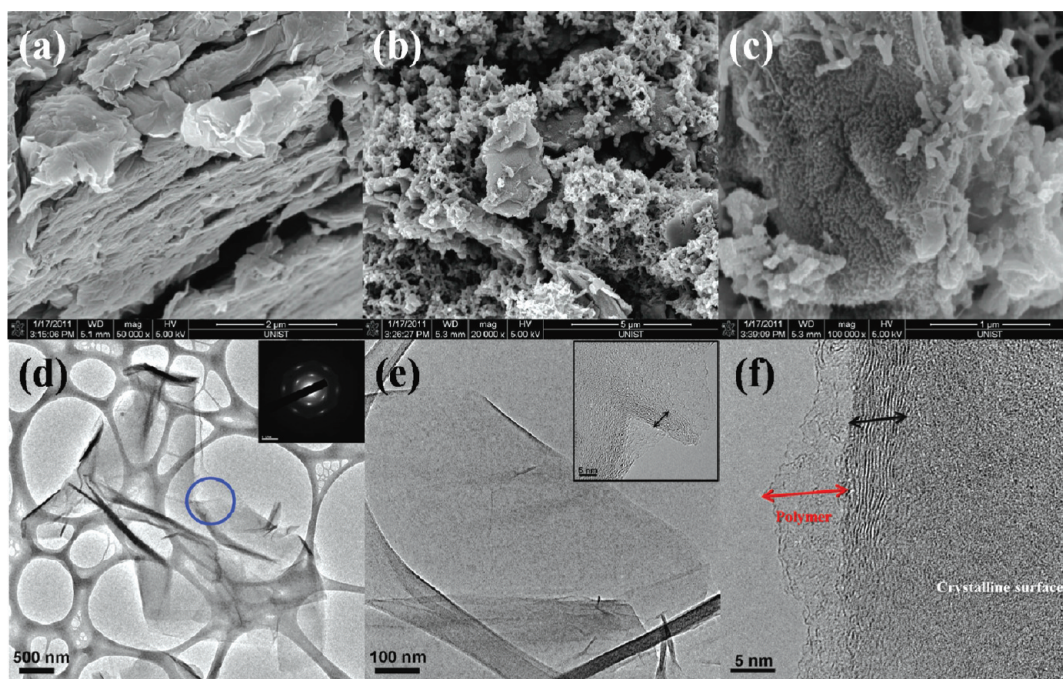
Figure 4. Typical FE-SEM images: (a) GO; (b and c) the surface of the PANi-*g*-rGO hybrid. HR-TEM images: (d) GO. Inset image is of a selected-area electron diffraction (SAED) pattern; (e) rGO-NH$_2$. Inset image is at higher magnification; (f) PANi-*g*-rGO.

final target hybrid indicates the presence of PANi in the samples.

The typical micromorphologies of the resulting GO and the hybrid PANi-*g*-rGO composite were observed by HR-TEM and FE-SEM, as exhibited in Figure 4.

A typical SEM image of the GO is given in Figure 4a, which shows the layer-by-layer structure in stacking with a size of tens of micrometers and the nanosheet morphologies. The FESEM images of the PANi-*g*-rGO hybrid show typical fibrillar morphology (Figure 4b and c), where in some areas the composites exhibit mainly an irregular morphology with multiple shapes including both fibrillar and a few rod-like structures. Also, graphene flakes can be seen embedded in the PANi, suggesting a graphene interconnection with the polymer network (see Figure S1a and c in the Supporting Information (SI)). These changes can be explained by the adsorption and intercalation of PANi on the surface and between the rGO sheets either sandwiched between rGO sheets or on the rGO surfaces (see Figure S1c in the SI).

It is well known that graphene is a good electron acceptor and aniline on the other hand is a very good electron donor.[44] When HCl is used as a dopant, therefore, the aniline monomer is likely to be absorbed onto the surface of GNS through electrostatic attraction and by the formation of weak charge-transfer complexes between the aniline monomer and the graphitic structure of GO. As a result of this absorption process, GO sheets are finely coated by PANi particles by the *in situ* polymerization of aniline monomer in the presence of GNS. Thus, it is aptly believed that the adsorption

probability of aniline monomers on the whole surface of graphene is equipotent, resulting in the formation of a continuous PANi coating on the surface of GO sheets. Hence, it is no wonder that the graphene nanosheets can be considered as a support material for PANi growth, providing a large number of active nucleation sites.

To obtain further insight into the nanosheet morphology of rGO and the hybrid as well as the layer structures including the layer exfoliation pattern, high-resolution transmission electron microscopy (HR-TEM) was used. HR-TEM images of GO exhibit a transparent layered and wrinkled silk-like structure, representing a curled and corrugated morphology intrinsically associated with graphene. This can be attributed to the disruption of the planar sp^2 carbon sheets by the introduction of sp^3-hybridized carbon upon oxidation, which is consistent with several previous reports. Interestingly, the TEM image (Figure 4d) showed a typical single-layer GO sheet with a lateral dimension of several micrometers, and the typical SAED pattern in the inset of Figure 4d confirms this phenomenon. After functionalization, however, tremendous changes in morphology reveal the introduction of aminophenol (Figure 4e) and PANi (Figure 4f) on the rGO surfaces. As for the PANi-*g*-rGO composite (Figure 4c), the coating of PANi is clearly visible, and it clearly distinguishes itself from the highly crystalline graphitic support, which is attributed to the surrounding of PANi on the rGO host. In addition, it could be seen that each flaky layer of the rGO uniformly piles up while layers of composite have individual directions due to the influence of PANi, indicating
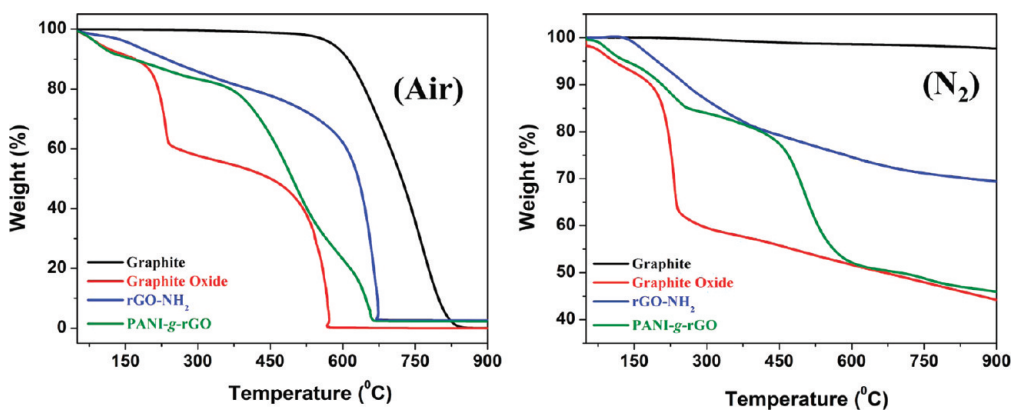
Figure 5. TGA thermograms of samples obtained with a ramping rate of 10 °C/min.
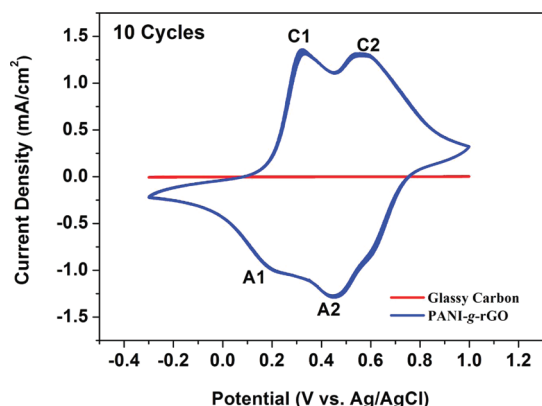
Figure 6. Cyclic voltammograms (CV) recorded in 1 M H$_2$SO$_4$ solution as the electrolyte at a sweep rate of 100 mV/s.

that the *in situ* polymerization affects the structure of rGO in an ordered way. Several high-resolution images at various magnifications are shown separately for clarification (see Figure S1d–S1i in the SI).

The comparisons of mass losses upon heating in nitrogen and air atmosphere as well as the content of the PANi covalently grafted to the GO (the degree of functionalization) were determined thermogravimetrically. As shown in Figure 5, the pristine graphite was thermally the most stable in both air and nitrogen, not showing any decomposition in the temperature ranges 50–600 and 50–900 °C, respectively, as expected. However, GO is thermally unstable, and exhibits pyrolysis of labile oxygen-containing functional groups, and acidic residues such as −OH, −CO, and −COO groups, leading to a major weight loss commencing at about 200 °C. This lowered thermal stability can also be ascertained to the reduced van de Waals interaction between the layers. Upon functionalization, the TGA patterns show typical stages of weight losses for the composite in both air and nitrogen atmospheres. The initial weight loss pattern of the PANi-*g*-rGO region around 130 °C is mainly assigned to the loss of bound water molecules from the structures, while the rapid loss in the second region at around 250 °C is attributed

to the oxidative degradation of the composite itself. As commonly observed,[45] PANi starts to decompose at a relatively low temperature less than 150 °C and is completely oxidized at about 660 °C, which is clearly evident. Interesting to note is that the char yields of those in air at 900 °C were almost nil for the PANi-*g*-rGO. The degree of functionalization from the gradual mass loss of the PANi-*g*-rGO in nitrogen suggests that around 50 mass % has been functionalized covalently. This increased thermal stability of the PANi-*g*-rGO composite could be due to the deposited PANi on the GO layers. Furthermore, the concomitant chemical reduction of GO during the preparation of rGO-NH$_2$ (thermal reduction) could also play an effective role in enhancing the thermal stability of the resulting rGO nanosheets, as evident from thermal stability of the hybrid as observed previously.[46]

The electrochemical performances of the PANi-*g*-rGO including its capacitative behavior were analyzed using cyclic voltammetry (CV) in 1 M H$_2$SO$_4$ with a potential range of −0.2 and 1 V *versus* Ag/AgCl at various scan rates. The capacitance estimated from the CV curve was reported by integrating over the CV curve to determine the average value of the area for one cycle.[47] A remarkable difference of electrochemical surface activity among the bare glassy carbon (GC) and the PANi-*g*-rGO recorded at a scan rate of 100 mV/s can be easily recognized from the representative CV curve shown in Figure 6.

As can be seen in Figure 6, there was no peak originating from the bare GC electrode, and it exhibits a negligibly low current density response. When compared with the GC electrode, however, the current density response and the CV loop area of the PANi-*g*-rGO electrode are both much larger, which clearly indicates that the electrochemical performance of the hybrid is remarkably enhanced owing to the addition of a PANi coating on the surface of the GO sheets. Two pairs of well-defined redox peaks appeared for the hybrids, which were attributed to two redox transitions of PANi, also suggesting the presence of pseudocapacitive PANi.[48] These peaks correspond to the redox

transitions between a semiconducting state (the leuco-emeraldine form) and a conducting state (polaronic emeraldine) designated as peaks C1/A1, and the Faradaic transformation of emeraldine to pernigraniline initiates the redox peaks C2/A2.[26] Interesting to note is that the CV loops have large rectangular areas with a capacitance of 250 F/g, indicating their potential as supercapacitors. From the CVs recorded for the composite at different scan rates, it was noticed that the cathodic peaks shift positively and the anodic peaks shift negatively with an increase of potential sweep rates from 10 to 200 mV/s (see Figure S3 in the SI). It should be noted that the synergetic effect resulting from the interactions of PANi and rGO may affect the shape and potential position of the CV curves, as clearly evident from our results. As exhibited in Figure S3, the CV curve of the PANi-*g*-rGO is close to being rectangular shaped at all scan rates, which might indicate that it possesses excellent electrical double-layer capacitance. Moreover, with increasing the sweep rate, the increase of specific capacitance is obvious without any distinctive changes in the shape of the CV profile. Additionally, all the CVs were quite stable for a number of cycles, and no significant current decrease was noticed in all cases, clearly indicating that the compound exhibited high cycling stability.

The electrical conductivity of PANi-*g*-rGO was determined on pressed pellets from powder by using a four-probe resistivity measurement system, and the average conductivities were collected. The value was found to be as high as 8.66 S/cm, which was stable and reproducible over a period of time, thereby indicating that the conductive networks in the system are good due probably to the covalent bonding between PANi and rGO.

CONCLUSION

Highly conducting polyaniline-grafted reduced graphene oxide (PANi-*g*-rGO) composites with enhanced properties were prepared in a facile and new route by functionalizing graphite oxide with 4-aminophenol *via* acyl chemistry, where a concomitant reduction of GO takes place. Simultaneous reduction of GO sheets and subsequent deprotection of the amine groups followed by an oxidative polymerization of aniline yielded a highly conducting PANi-grafted reduced graphene oxide composite (PANi-*g*-rGO). Initial changes in surface functionalities confirmed that PANi was covalently grafted to the reduced GO sheets, thus forming highly conductive networks. Electrical conductivity of these hybrid assemblies showed a value as high as 8.66 S/cm. Dramatic improvements in their properties have been described due to the synergistic effect between the two components. In addition to the merits in preparation, our composite showed more pronounced electrochemical performances than the pristine GO as supercapacitor electrodes, exhibiting a capacitance value of 250 F/g. These findings may have direct and important consequences for appealing technological applications in the field of optoelectronic devices and in sensing and catalysis as well.

METHODS

Materials. Flaky graphite powder (400 nm; 99.99% metal base; impurities (quartz + mica) < 0.1%, H_2O ~0.2%) was obtained from Nanostructured & Amorphous Materials Inc., Houston, TX, USA. Reagent-grade aniline as a monomer (stored at 0 °C) and *N-Boc*-4-aminophenol and ammonium peroxydisulfate (($NH_4)_2S_2O_8$) (APS) were purchased from Sigma-Aldrich and used as received. Dry tetrahydrofuran (THF) and thionyl chloride from Aldrich were distilled prior to usage. All other solvents were used as received unless otherwise stated.

Synthesis of PANi-g-rGO by Chemical Grafting of N-Boc-4-Aminophenol with GO. Initially graphite oxide was prepared by a modified Hummers and Offeman method as described as follows. Graphite (3 g) was mixed with 1.5 g of $NaNO_3$ and 75 mL of concentrated H_2SO_4. The mixture was cooled to 0 °C in an ice bath and stirred for 2 h. Then, 9 g of $KMNO_4$ was added slowly (temperature was maintained at <5 °C throughout the mixing) and continuously stirred for another hour. The cooling bath was then removed and the mixture was cooled to room temperature. To this was added ~100 mL of distilled water (gas evolved), and the temperature was increased to 90 °C in an oil bath. After reaching 90 °C, 300 mL of water was added again and the solution was continuously stirred for another hour and a half. The color of the mixture turned to mud brown. This mixture was then treated with 30 mL of 30% H_2O_2, and ~3 L of hot water was added to dilute the mixture. The mixture was further washed with excess water until the pH of the filtrate was nearly neutral

and then vacuum filtered and freeze-dried under reduced pressure overnight to yield GO. This material was used for further reactions.

Briefly, 500 mg of GO was treated with excess amount of $SOCl_2$ (20 mL) under a nitrogen atmosphere for 24 h under reflux, to convert the surface-bound carboxylic acids to acyl chlorides. After reflux, the residual $SOCl_2$ was removed by distillation under reduced pressure, and the obtained solids were immediately dispersed in anhydrous THF and further reacted with *N-Boc*-4-aminophenol in nitrogen atmosphere for 12 h. The N-*Boc* groups were then deprotected by washing with trifluoroacetic acid, and the resulting mixture was subsequently separated by centrifugation, washed well with methanol, and freeze-dried under reduced pressure overnight to yield amine-terminated reduced GO, designated as rGO-NH_2.

Polyaniline-grafted rGO (PANi-*g*-rGO) was simply prepared *via* an *in situ* polymerization of aniline as a monomer in the presence of rGO-NH_2. The detailed procedure is as follows: the rGO-NH_2 was first dispersed in 10 mL of 1 N HCl and ultrasonicated for about 30 min to obtain a homogeneous dispersion. This suspension was cooled in an ice bath to 0 °C. Then, aniline monomer (0.5 mL) was added to the rGO-NH_2 suspension with continuous stirring, after which, a freshly prepared solution of 1.14 g of the oxidant (($NH_4)_2S_2O_8$ in 10 mL of water was slowly added while stirring in cool conditions. A few minutes later the dark suspension became green, indicating a good initiation of polymerization, and then the reaction was

continued for another 5 h, where the ice bath was maintained to ensure proper polymerization. The resulting dark green material was filtered after washing with HCl to remove any unreacted monomer and oxidant. It was then washed several times with deionized water and acetone followed by freeze-drying under reduced pressure overnight to yield PANi-*g*-rGO.

Instrumentation. The crystallographic structures of the materials were determined by a wide-angle X-ray diffraction system (Rigaku RU-200 diffractometer) equipped with Ni-filtered Cu Kα radiation (40 kV, 100 mA, λ = 0.15418 nm). While the initial changes in the surface chemical bonding as well as the covalent grafting behavior of the hybrids were recorded by Fourier transformed infrared spectrophotometry (FT-IR, Perkin-Elmer Spectrum GX, s100, USA) in the frequency range 4000−450 cm^{-1}, Raman spectra and images for the samples were obtained with a micro-Raman system (Alpha 300s, WITec GmbH) with 532 nm lasers. In order to avoid the laser-induced thermal effects or damage to the samples, the incident laser power was controlled to be less than 4 mW. X-ray photoelectron spectroscopy measurements were carried out using a Thermo Fisher K-alpha spectrometer employing monochromatic Al Kα radiation as the X-ray source. The content of the polymer and the decomposition patterns were determined thermogravimetrically using a TGA analyzer (Q200, TA Instruments, USA) at a ramp rate of 10 °C min^{-1} in both nitrogen and air atmosphere. Microstructure and structural morphologies of the hybrids were investigated by a field emission scanning electron microscopy (FE-SEM), performed on a LEO 1530FE and FEI NanoSem 200. High-resolution transmission electron microscopic (HR-TEM) images were obtained for all samples using a JEOL JEM-2100F microscope at an accelerating voltage of 200 kV. Composites pressed to tablets under a hydraulic press to a mirror finish were subjected to the standard four-point probe method at ambient temperature (Advanced Instrument Technology CMT-SR1000N with Jandel Engineering probe), which provided information on sheet resistance and the electrical conductivity. Factory-recommended correction factors were used to calculate the conductivity values, which were the averages of a few measurements of the same pressed film.

Electrochemical Properties. For the electrochemical measurements, cyclic voltammetry was carried out using a VersaSTAT3 AMETEK model (Princeton Applied Research TN) potentiostat/galvanostat employing a standard three-electrode electrochemical cell that consisted of a composite loaded glassy carbon as the working electrode, Ag/AgCl as the reference electrode, and platinum gauze as the counter electrode. Glassy carbon electrodes (GCE) of 3.0 mm in diameter were polished with finer emery paper and 0.3 μm Al$_2$O$_3$ powder. This working electrode was cleaned in an ultrasonic bath for 1 min and dried in air for use. In a typical process for composite loading, PANi-*g*-rGO was dispersed in NMP with 0.2 mL of Nafion solution and sonicated in an ultrasonic bath for 5 min to get a homogeneous solution. Then, about 30−40 μL of the mixture was coated on GCE and dried in air at 60 °C for 5 min. Electrochemical experiments were carried out at room temperature in 1 M aqueous H$_2$SO$_4$ solution as the electrolyte. All potentials are reported relative to an Ag/AgCl (saturated KCl) reference electrode at different scan rates, and the potential window for cycling was confined between −0.3 and 1 V.

Conflict of Interest: The authors declare no competing financial interest.

Supporting Information Available: Morphology images of higher magnification including FESEM and HRTEM images and CV curves for the sample obtained at different scan rates are presented. This material is available free of charge *via* the Internet at http://pubs.acs.org.

REFERENCES AND NOTES

1. Rao, C. N. R.; Sood, A. K.; Subrahmanyam, K. S.; Govindaraj, A. Graphene: The New Two-Dimensional Nanomaterial. *Angew. Chem., Int. Ed.* **2009**, *48*, 7752–7777.
2. Allen, M. J.; Tung, V. C.; Kaner, R. B. Honeycomb Carbon: A Review of Graphene. *Chem. Rev.* **2010**, *110*, 132–145.
3. Simon, P.; Gogotsi, Y. Materials for Electrochemical Capacitors. *Nat. Mater.* **2008**, *7*, 845–854.
4. Ramanathan, T; Abdala, A. A.; Stankovich, S.; Dikin, D. A.; Herrera Alonso, M.; Piner, R. D.; Adamson, D. H.; Schniepp, H. C.; Chen, X; Ruoff, R. S.; *et al.* Functionalized Graphene Sheets for Polymer Nanocomposites. *Nat. Nanotechnol.* **2008**, *3*, 327–331.
5. Stankovich, S.; Dikin, D. A.; Dommett, G. H. B.; Kohlhaas, K. M.; Zimney, E. J.; Stach, E. A.; Piner, R. D.; Nguyen, S. T.; Ruoff, R. S. Graphene-Based Composite Materials. *Nature* **2006**, *442*, 282–286.
6. Pumera, M.; Ambrosi, A.; Bonanni, A.; Chng, E. L. K.; Poh, H. L. Graphene for Electrochemical Sensing and Biosensing. *TrAC Trends Anal. Chem.* **2010**, *29*, 954–965.
7. Arico, A. S.; Bruce, P.; Scrosati, B.; Tarascon, J. M.; Van Schalkwijk, W. Nanostructured Materials for Advanced Energy Conversion and Storage Devices. *Nat. Mater.* **2005**, *4*, 366–377.
8. Liu, C. J.; Burghaus, U.; Besenbacher, F.; Wang, Z. L. Preparation and Characterization of Nanomaterials for Sustainable Energy Production. *ACS Nano* **2010**, *4*, 5517–5526.
9. Pumera, M. Graphene-Based Nanomaterials for Energy Storage. *Energy Environ. Sci.* **2011**, *4*, 668–674.
10. Liang, M.; Zhi, L. Graphene-Based Electrode Materials for Rechargeable Lithium Batteries. *J. Mater. Chem.* **2009**, *19*, 5871.
11. Wang, C.; Li, D.; Too, C. O.; Wallace, G. G. Electrochemical Properties of Graphene Paper Electrodes Used in Lithium Batteries. *Chem. Mater.* **2009**, *21*, 2604–2606.
12. Vivekchand, S.; Rout, C.; Subrahmanyam, K.; Govindaraj, A.; Rao, C. Graphene-Based Electrochemical Supercapacitors. *J. Chem. Sci.* **2008**, *120*, 9–13.
13. Zhang, L. L.; Zhou, R.; Zhao, X. S. Graphene-Based Materials as Supercapacitor Electrodes. *J. Mater. Chem.* **2010**, *20*, 5983–5992.
14. Wang, Y.; Shi, Z.; Huang, Y.; Ma, Y.; Wang, C.; Chen, M.; Chen, Y. Supercapacitor Devices Based on Graphene Materials. *J. Phys. Chem. C* **2009**, *113*, 13103–13107.
15. Yoo, J. J.; Balakrishnan, K.; Huang, J.; Meunier, V.; Sumpter, B. G.; Srivastava, A.; Conway, M.; Mohana Reddy, A. L.; Yu, J.; Vajtai, R.; *et al.* Ultrathin Planar Graphene Supercapacitors. *Nano Lett.* **2011**, *11*, 1423–1427.
16. Cai, D.; Song, M. Recent Advance in Functionalized Graphene/Polymer Nanocomposites. *J. Mater. Chem.* **2010**, *20*, 7906–7915.
17. Long, Y.-Z.; Li, M.-M.; Gu, C.; Wan, M.; Duvail, J.-L.; Liu, Z.; Fan, Z. Recent Advances in Synthesis, Physical Properties and Applications of Conducting Polymer Nanotubes and Nanofibers. *Prog. Polym. Sci.* **2011**, *36*, 1415–1442.
18. Nyholm, L.; Nyström, G.; Mihranyan, A.; Strømme, M. Toward Flexible Polymer and Paper-Based Energy Storage Devices. *Adv. Mater.* **2011**, *23*, 3751–3769.
19. Geniès, E. M.; Boyle, A.; Lapkowski, M.; Tsintavis, C. Polyaniline: A Historical Survey. *Synth. Met.* **1990**, *36*, 139–182.
20. Dhand, C.; Das, M.; Datta, M.; Malhotra, B. D. Recent Advances in Polyaniline Based Biosensors. *Biosen. Bioelectron.* **2011**, *26*, 2811–2821.
21. Snook, G. A.; Kao, P.; Best, A. S. Conducting-Polymer-Based Supercapacitor Devices and Electrodes. *J. Power Sources* **2011**, *196*, 1–12.
22. Liu, C.; Li, F.; Ma, L. P.; Cheng, H. M. Advanced Materials for Energy Storage. *Adv. Mater.* **2010**, *22*, E28–E62.
23. Kaskhedikar, N. A.; Maier, J. Lithium Storage in Carbon Nanostructures. *Adv. Mater.* **2009**, *21*, 2664–2680.
24. Gómez, H.; Ram, M. K.; Alvi, F.; Villalba, P.; Stefanakos, E.; Kumar, A. Graphene-Conducting Polymer Nanocomposite as Novel Electrode for Supercapacitors. *J. Power Sources* **2011**, *196*, 4102–4108.

25. Wang, H.; Hao, Q.; Yang, X.; Lu, L.; Wang, X. Graphene Oxide Doped Polyaniline for Supercapacitors. *Electrochem. Commun.* **2009**, *11*, 1158–1161.

26. Wang, D.-W.; Li, F.; Zhao, J.; Ren, W.; Chen, Z.-G.; Tan, J.; Wu, Z.-S.; Gentle, I.; Lu, G. Q.; Cheng, H.-M. Fabrication of Graphene/Polyaniline Composite Paper *via In Situ* Anodic Electropolymerization for High-Performance Flexible Electrode. *ACS Nano* **2009**, *3*, 1745–1752.

27. Yan, J.; Wei, T.; Shao, B.; Fan, Z.; Qian, W.; Zhang, M.; Wei, F. Preparation of a Graphene Nanosheet/Polyaniline Composite with High Specific Capacitance. *Carbon* **2010**, *48*, 487–493.

28. Hummers, W. S.; Offeman, R. E. Preparation of Graphitic Oxide. *J. Am. Chem. Soc.* **1958**, *80*, 1339–1339.

29. Zu, S.-Z.; Han, B.-H. Aqueous Dispersion of Graphene Sheets Stabilized by Pluronic Copolymers: Formation of Supramolecular Hydrogel. *J. Phys. Chem. C* **2009**, *113*, 13651–13657.

30. Kumar, N. A.; Jeong, Y. T. Fabrication of Conducting Polyaniline-Multiwalled Carbon Nanotube Nanocomposites and Their Use as Templates for Loading Gold Nanoparticles. *Polym. Int.* **2010**, *59*, 1367–1374.

31. Špitalsk, Z.; Danko, M.; Mosnáček, J. Preparation of Functionalized Graphene Sheets. *Curr. Org. Chem.* **2011**, *15*, 1133–1150.

32. Titelman, G. I.; Gelman, V.; Bron, S.; Khalfin, R. L.; Cohen, Y.; Bianco-Peled, H. Characteristics and Microstructure of Aqueous Colloidal Dispersions of Graphite Oxide. *Carbon* **2005**, *43*, 641–649.

33. Xu, J.; Wang, K.; Zu, S.-Z.; Han, B.-H.; Wei, Z. Hierarchical Nanocomposites of Polyaniline Nanowire Arrays on Graphene Oxide Sheets with Synergistic Effect for Energy Storage. *ACS Nano* **2010**, *4*, 5019–5026.

34. Wan, M.; Li, M.; Li, J.; Liu, Z. Structure and Electrical Properties of the Oriented Polyaniline Films. *J. Appl. Polym. Sci.* **1994**, *53*, 131–139.

35. Malard, L. M.; Pimenta, M. A.; Dresselhaus, G.; Dresselhaus, M. S. Raman Spectroscopy in Graphene. *Phys. Rep.* **2009**, *473*, 51–87.

36. Liu, S.; Liu, X. H.; Li, Z. P.; Yang, S. R.; Wang, J. Q. Fabrication of Free-Standing Graphene/Polyaniline Nanofibers Composite Paper *via* Electrostatic Adsorption for Electrochemical Supercapacitors. *New J. Chem.* **2011**, *35*, 369–374.

37. Gupta, A.; Chen, G.; Joshi, P.; Tadigadapa, S.; Eklund Raman Scattering from High-Frequency Phonons in Supported n-Graphene Layer Films. *Nano Lett.* **2006**, *6*, 2667–2673.

38. Graf, D.; Molitor, F.; Ensslin, K.; Stampfer, C.; Jungen, A.; Hierold, C.; Wirtz, L. Spatially Resolved Raman Spectroscopy of Single- and Few-Layer Graphene. *Nano Lett.* **2007**, *7*, 238–242.

39. Chen, W.; Yan, L.; Bangal, P. R. Chemical Reduction of Graphene Oxide to Graphene by Sulfur-Containing Compounds. *J. Phys. Chem. C* **2010**, *114*, 19885–19890.

40. Zhang, K.; Zhang, L. L.; Zhao, X. S.; Wu, J. S. Graphene/Polyaniline Nanofiber Composites as Supercapacitor Electrodes. *Chem. Mater.* **2010**, *22*, 1392–1401.

41. Yang, Y.; Wan, M. Chiral Nanotubes of Polyaniline Synthesized by a Template-Free Method. *J. Mater. Chem.* **2002**, *12*, 897–901.

42. Jeon, I.-Y.; Yu, D.; Bae, S.-Y.; Choi, H.-J.; Chang, D. W.; Dai, L.; Baek, J.-B. Formation of Large-Area Nitrogen-Doped Graphene Film Prepared from Simple Solution Casting of Edge-Selectively Functionalized Graphite and Its Electrocatalytic Activity. *Chem. Mater.* **2011**, *23*, 3987–3992.

43. Wang, H.; Hao, Q.; Yang, X.; Lu, L.; Wang, X. A Nanostructured Graphene/Polyaniline Hybrid Material for Supercapacitors. *Nanoscale* **2010**, *2*, 2164–2170.

44. Vallés, C.; Jiménez, P.; Muñoz, E.; Benito, A. M.; Maser, W. K. Simultaneous Reduction of Graphene Oxide and Polyaniline: Doping-Assisted Formation of a Solid-State Charge-Transfer Complex. *J. Phys. Chem. C* **2011**, *115*, 10468–10474.

45. Gheno, G.; de Souza Basso, N. R.; Hübler, R. Polyaniline/Graphite Nanocomposites: Synthesis and Characterization. *Macromol. Symp.* **2011**, *299−300*, 74–80.

46. Xu, L. Q.; Liu, Y. L.; Neoh, K.-G.; Kang, E.-T.; Fu, G. D. Reduction of Graphene Oxide by Aniline with Its Concomitant Oxidative Polymerization. *Macromol. Rapid Commun.* **2011**, *32*, 684–688.

47. Kumar, N. A.; Jeon, I. Y.; Sohn, G. J.; Jain, R.; Kumar, S.; Baek, J. B. Highly Conducting and Flexible Few-Walled Carbon Nanotube Thin Film. *ACS Nano* **2011**, *5*, 2324–2331.

48. Wang, Y. G.; Li, H. Q.; Xia, Y. Y. Ordered Whiskerlike Polyaniline Grown on the Surface of Mesoporous Carbon and Its Electrochemical Capacitance Performance. *Adv. Mater.* **2006**, *18*, 2619–2623.